AIMS Materials Science, 9(4): 604–616.
DOI: 10.3934/matersci.2022036
Received: 11 March 2022
Revised: 14 June 2022
Accepted: 27 June 2022
Published: 4 August 2022

http://www.aimspress.com/journal/Materials

Research article

Effect of titanium addition on sub-structural characteristics of low carbon copper bearing steel in hot rolling

ME Makhatha*

University of Johannesburg, Faculty of Engineering and the Built Environment, Department of Engineering Metallurgy, Johannesburg, 2028, South Africa

* **Correspondence:** Email: emakhatha@uj.ac.za; Tel: +011-559-6182.

Abstract: The low carbon copper-bearing steel exhibits high toughness and better weldability. In the present investigation, 0.05C–1.52Cu–1.45Mn stainless steel and its titanium added counterpart which is 0.05C–0.05Ti–1.52Cu–1.45Mn stainless steel were subjected to hot rolling. The hot rolling test followed by quenching to retain the microstructure was done using a hot-rolling mill. The rolling was done at two different temperatures of 800 ℃ and 850 ℃. The characterization of microstructure was done using electron back scattered diffraction and transmission electron microscopy analysis. The 0.05C–1.52Cu–1.45Mn stainless steel when subjected to hot rolling at a lower temperature envisaged a deformed microstructure rather transformed one. However, the same steel at a higher temperature envisages a transformed microstructure. There was no variation in hardness was observed. However, the addition of 0.05 wt% of titanium in 0.05C–1.52Cu–1.45Mn stainless steel influenced the softening and the microstructure showed some recrystallization; the hardness was decreased with the increasing rolling temperature because the solubility of titanium in the austenite phase increased with temperature which leads to suppression austenitic grain/sub-grain growth and hardness. The mean sub-grain size for 0.05C–1.52Cu–1.45Mn stainless steel was 2.75 μm. However, the addition of titanium leads to a decrease in the mean sub-grain size. A marginally larger mean sub-grain size was observed when 0.05C–0.05Ti–1.52Cu–1.45Mn stainless steel was rolled at a higher temperature. A comparatively finer precipitate of copper, titanium and oxy-silicates of Ferrous/Manganese in order of nanometer was formed during rolling at a higher temperature.

Keywords: hot rolling; subgrains; misorientation angle; precipitation; hardness

Abbreviations: EBSD: Electron backscattered diffraction; OES: Optical emission spectroscopy; TEM: Transmission emission microscopy

1. Introduction

The low carbon content steel exhibits high toughness and better weldability due to low carbon content. The addition of micro-alloy elements to low carbon steel is a widely used technique to improve the microstructure. An element such as copper improves the strength significantly while keeping the desired toughness and weldability. It was reported that the addition of copper in low carbon steel improves the strength via precipitation strengthening [1–5]. In context to copper addition, the strength can be improved by adding elements like Ti and Mo which formed tiny carbides and nitrides which hinders the movement of the dislocations and leads to further increase the strength. However, the addition of such elements requires an optimized thermomechanical processing route and controlled cooling to achieve desired microstructural properties [6]. The thermo-mechanical processing of low carbon steel is one of the widely used techniques to advance the microstructure and mechanical properties. The hot rolling of such steel involved the plastic deformation along with thermal cycling to produced fine grain microstructure and at the same time, it induces strength and desire toughness [7,8]. The process parameters such as rolling temperature and percent reduction in thickness of rolled strips envisage microstructure improvement. During hot rolling, the microstructure undergoes straining which produced dislocations; however, during cooling, the restoration mechanism (recovery/recrystallization) described the quenched microstructure. The restoration mechanics can be dynamic/static depending upon whether the nucleation and growth or annihilation of dislocations take place during deformation or after the deformation [9,10]. The distribution of crystal orientation also plays a significant role in deciding the final microstructure [11]. It was reported that the hot rolled low carbon steel exhibits a random texture because of shorted re-crystallization time [11]. Funkawa et al., investigated that the hot rolling process envisages precipitation of different fine carbide phases which leads to improving the mechanical strength of the materials [12]. In context to the addition of micro-alloying elements for strengthening, Misra et al., also studied the microstructure of copper-bearing steel during hot rolling; they reported that the addition of copper increased the strength by 25 MPa [13]. They also reported the presence of nano-sized copper precipitated and other carbides ad nitrides in hot rolled steel. Hwang et al also investigated the correlation of microstructure and mechanical properties of thermomechanical processed low carbon steel. During electron backscattered diffraction (EBSD) analysis, they found that the grain size of lower bainite (LB) and lath martensite (LM) microstructures was relatively smaller than the granular bainite (GB) or degenerate upper bainite (DUB) microstructure [14]. It is also important to understand that, during hot rolling of micro-alloyed low carbon steel, the sub-structures/sub-grains are also generated during deformation/straining. The characteristics of such sub-grains are also important to characterize the microstructure. The sub-grain characteristics will be influenced by the restoration mechanism during hot deformation and/or after the deformation that is colling. These sub-grains can be formed in the grain interior or along the grain boundaries (high energy sites). The characteristics of such sub-grains were reported by Kumar et al., during thermos-mechanical processing of duplex stainless steel [15,16]. However, such characteristics of sub-grains are not reported to date for low carbon copper bearing steel. In the present work, the characteristics of such sub-grain that formed during hot rolling was studied. In addition to this, a titanium micro-alloyed counterpart of copper-bearing low carbon steel was also studied and the influence of titanium on the microstructure was investigated during hot rolling.

2. Materials and methods

There were two different alloys (alloy-1 and alloy-2) used in the present investigation. The

chemical composition of alloy-1 and alloy-2 is shown in tables 1 and 2, respectively. The microalloying element titanium (in wt% of 0.05) was added to alloy-2 complementary to the composition used in alloy-1. The standard procedure of steel casting was followed using a 7 kg of charge in an induction furnace. The chemical compositing of steel was calculated using optical emission spectroscopy (OES). To achieve such desired compositing, the chemical composition of the metal pool (during casting) was tested multiple times using OES which provided an idea of the required wt% of microalloying elements which was added to the hot metal pool. The Zirconia crucible was used to avoid any carbon pic-up during the casting process and the final chemical composition was calculated using optical emission spectroscopy. To seal any minor cracks and empty spaces in casted steel, the material was subjected to forging operation using a pneumatic hammer of 0.5 t capacity. The forging temperature was 1050 ℃ with a soaking time of 6 h. The hot rolling test followed by quenching to retain the microstructure was done using a hot-rolling mill. The rolling was done at two different temperatures of 800 ℃ and 850 ℃. The Vickers microhardness test with a diamond intender was used to calculate the microhardness of the samples. The applied load was 0.1 kg with a dwell time of 15 s. The sample for microhardness testing was made using a diamond cutter grinding machine and surface polishing was done using emery paper. The polishing was done from coarse to fine grit size of emery paper. The sample mounting was done to make the surface in contact to be flat with the diamond intender during microhardness testing. The microstructural investigations were accomplished by means of electron backscattered diffraction (EBSD) operated at an accelerating voltage of 20 kV. The occupied distance was 12 mm in the high current mode with an aperture size of 60 μm. The step size of 0.4 μm was used to acquire EBSD maps. The samples for EBSD were prepared by standard mechanical polishing using a TEGRAPOL polishing machine. The grit size was used in the size sequence of 9 μ, 3 μ and 1 μ. There was no etching done on the sample for EBSD characterization. The post-processing of EBSD maps was done using HKL Technology channel 5 Software. The substructural studies were also made by transmission electron microscopy characterization. In context to characterize the sub-grains/dislocations, a transmission emission microscopy (TEM) technique was used. The samples were made by standard mechanical polishing required for TEM characterizations.

Table 1. Chemical composition of alloy-1.

Element	Weight (%)
C	0.05
Cu	1.52
Mn	1.45
Si	0.12
P	0.01
S	0.01
Fe	balance

Table 2. Chemical composition of alloy-2.

Element	Weight (%)
C	0.05
Cu	1.52
Mn	1.45
Si	0.12
P	0.01
S	0.02
Ti	0.05
Fe	balance

3. Results and discussion

3.1. Hardness

The Vickers microhardness for samples of alloy-1 and alloy-2 which were subjected to rolling at a temperature of 800 ℃ and 850 ℃ is shown in Figure 1. The alloy-2 containing titanium as a micro-alloyed element exhibited higher hardness as compared to its counterpart alloy without having titanium (alloy-1). The addition of titanium in low carbon stainless steel influences the softening kinetics of quenched microstructure. There was a possibility of hard titanium carbide/nitride precipitates formation, however, it is to be confirmed from the microstructure. The microhardness of alloy-2 was decreased with an increasing rolling temperature because the solubility of titanium in the austenite phase increased with temperature which results in to decrease in the possibility of titanium carbide/nitride formation and further suppressing the austenitic grain/sub-grain growth and hardness. In context to solubility, the higher rolling temperature envisages a greater degree of softening.

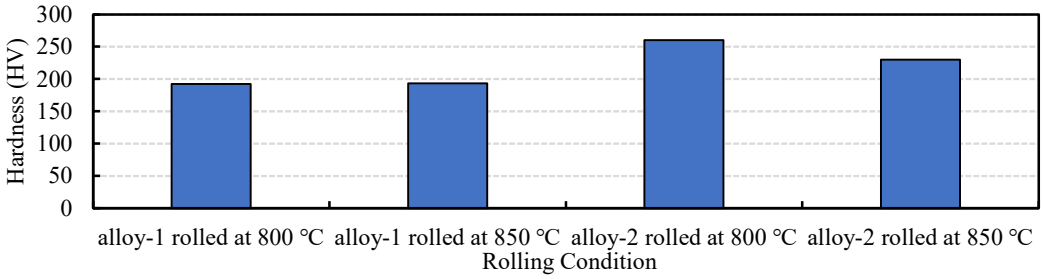

Figure 1. Hardness value for alloy-1 and alloy-2 when the samples rolled at a temperature of 800 ℃ and 850 ℃ respectively.

3.2. Sub-grain size

When samples were rolled at a lower temperature (of 800 ℃), this temperature was supposed to be below Ar3 temperature and it was ferrite/two-phase region which envisage work hardening/warm working. Hence the quenched microstructure was a deformed microstructure rather than a transformed one. However, when the samples were rolled at a higher temperature (of 850 ℃) which was above Ar3 temperature; the microstructure during hot rolling was most likely austenite; however, it is important to understand that the deformed austenite may be fine-grained or large-grained depending upon hot rolling parameters. The quenching envisages a phase transformation leading to the elimination of deformed microstructure. When the alloy-1 underwent hot rolling at a lower temperature of 800 ℃, it showed mostly the deformed microstructure which is depicted in Figure 2a. However, when the rolling temperature was increased, the transformed microstructure showed some recrystallized grain along with equiaxed grains as shown in Figure 2b. The Figure 2c shows microstructure when the alloy-2 samples rolled at a lower temperature of 800 ℃, it was clear from the microstructure that is exhibited deformed grains with elongated grain boundaries (along the rolling direction), however when the same sample was subjected to hot-rolled at a higher temperature, it showed transformed microstructure with some of the equiaxed grains which are shown in Figure 2d. In addition to the equiaxed microstructure; few of the recrystallized grains were also visible. It is suggested that these recrystallized grains were formed due to the restoration of deformed microstructure which was generated during the rolling

process. The EBSD orientation map is depicted different orientations as a function of color, the same color represents the same grain orientation.

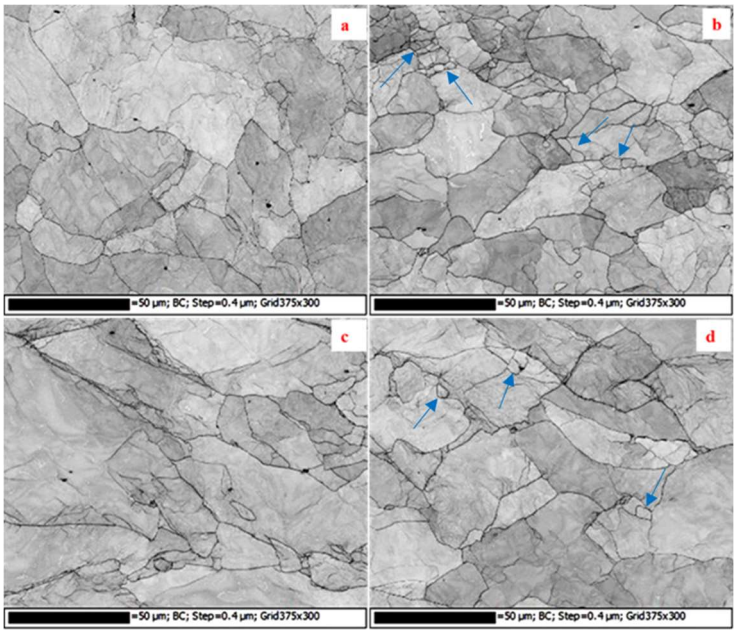

Figure 2. EBSD image at a step size 0.4 µm showing band contrast for (a) alloy-1 rolled at a temperature of 800 ℃; (b) alloy-1 rolled at a temperature of 850 ℃, the recrystallized grains are shown by blue arrows; (c) alloy-2 rolled at a temperature of 800 ℃ and (d) alloy-2 rolled at a temperature of 850 ℃, the recrystallized grains are shown by blue arrows.

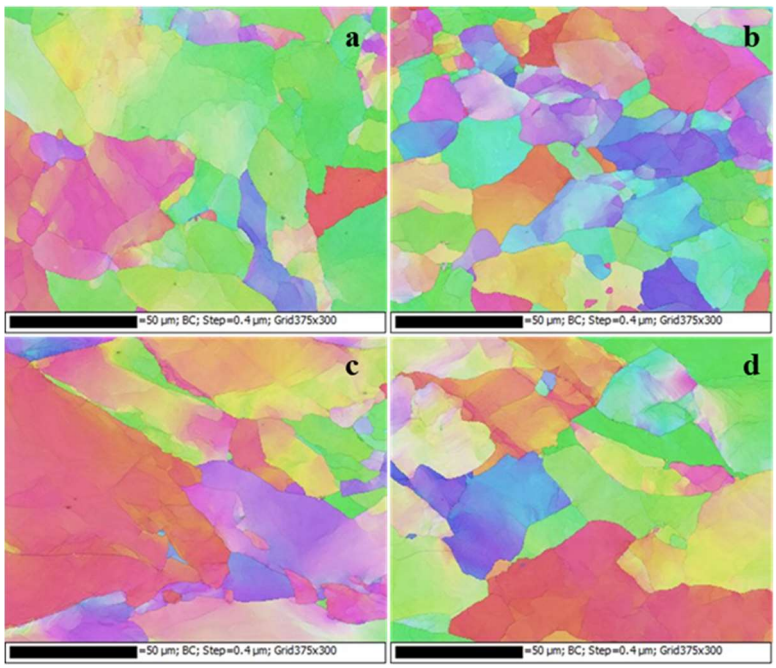

Figure 3. EBSD orientation map for (a) alloy-1 rolled at a temperature of 800 ℃ (b) alloy-1 rolled at a temperature of 850 ℃; (c) alloy-2 rolled at a temperature of 800 ℃ and (d) alloy-2 rolled at a temperature of 850 ℃.

The subgrain size was calculated using HKL Channel 5 software associated with EBSD phase maps. The measurement of subgrain was considered within the field of view and entire EBSD scanned area as shown in Figure 2. The beam scanning point-by-point mode was designed for such a sampling strategy. The substructure having a misorientation angle of less than 10° considered over the entire field of view defines a subgrain. The intercept graph (in channel 5 software) was plotted and its mean value provided the "mean subgrain size" over the entire field of view. A minimum of 55 subgrains were considered for calculating the mean subgrain size. The step size of 0.4 μm was used to acquire EBSD maps; therefore, all the subgrains either equal to or larger than a size of 0.4 μm were considered for the entire field of view. The mean sub-grain size of the alloy-1 was larger than its titanium micro-alloyed counterpart (alloy-2) as shown in Figure 4. The addition of titanium leads to a reduction in the mean sub-grain size from 2.75 μm to 2.31 μm when the samples were rolled at a lower temperature. As the sub-grain behaves like a grain in the microstructure, therefore the addition of titanium leads to the creation of finer sub-grains in the microstructure. However, a marginally larger average sub-grain size was observed when alloy-2 was rolled at a temperature of 850 ℃ as shown in Figure 4. It was mainly due to the difference in deformed stated and transformed state softening.

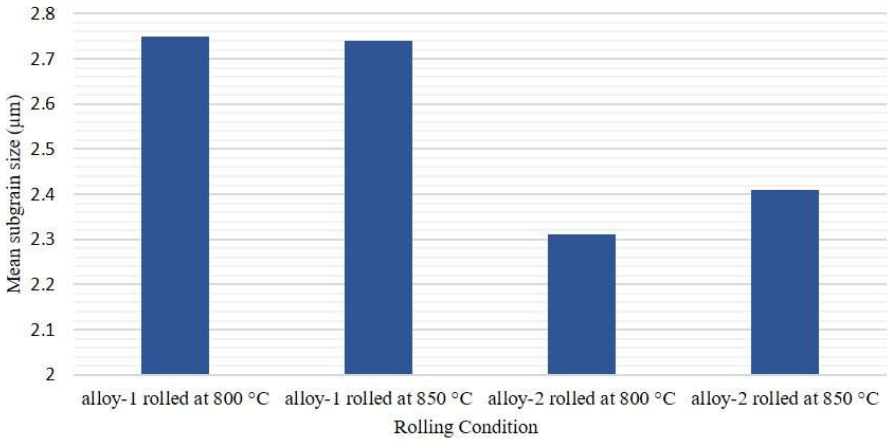

Figure 4. Mean sub-grain size for alloy-1 and alloy-2 when the samples rolled at a temperature of 800 ℃ and 850 ℃, respectively.

3.3. Misorientation angle distribution

The mean low angle boundaries misorientation (in degree) was calculated using HKL Channel 5 software associated with "EBSD phase maps" (Figure 2) as shown in Figure 5. EBSD image at a step size of 0.4 μm for misorientations greater than 5° is shown in Figure 6. The misorientation above 10° was considered "high angle boundary misorientation" and less than 10° was considered "low angle boundary misorientation". The fractions of misorientations in the range of 0° to 60° were calculated for all samples using HKL Channel 5 software as shown in Figure 7 which included both the "high angle grain boundaries" and "low angle grain boundaries". The "mean low angle boundaries misorientation" was obtained by calculating the mean of fractions misorientation less than 10° considering the entire scanned area of EBSD phase maps (Figure 2). The mean low angle grain boundaries misorientation for alloy-1 is lower than that of alloy-2 for both the rolling temperatures (800 ℃ and 850 ℃) as shown in Figure 5. However, the EBSD image at a step size of 0.4 μm for misorientations greater than 5° is shown in Figure 6. The deformed microstructure for both the alloy

is shown in Figure 6a,c. The deformed microstructure was elongated along the rolling direction and very minimal recrystallization was observed. The same was also reported in earlier section Figure 2 of section 3.2. However, the alloy-1 and 2, depicted some of the recrystallized grains surrounded with sub-grains which is shown in Figure 6 b,d, respectively. This evidence is conclusive as the same was observed earlier (section 3.2).

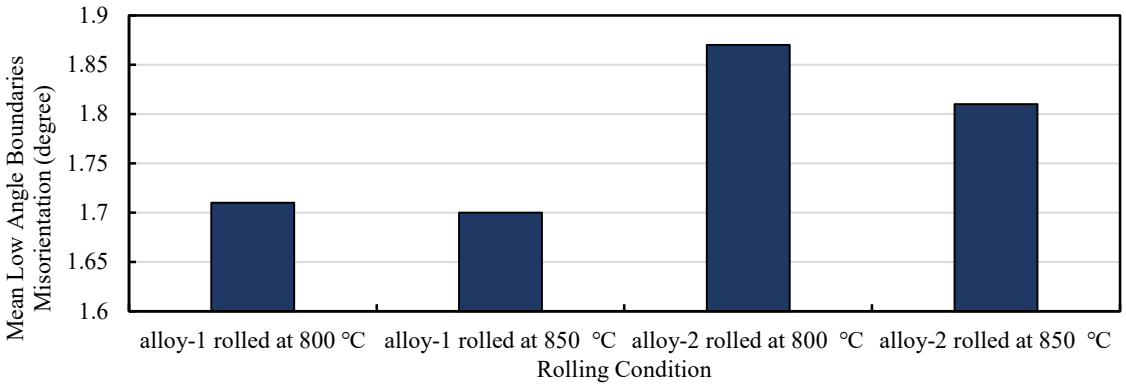

Figure 5. Mean low angle boundaries misorientation for alloy-1 and alloy-2 when the samples rolled at a temperature of 800 ℃ and 850 ℃, respectively.

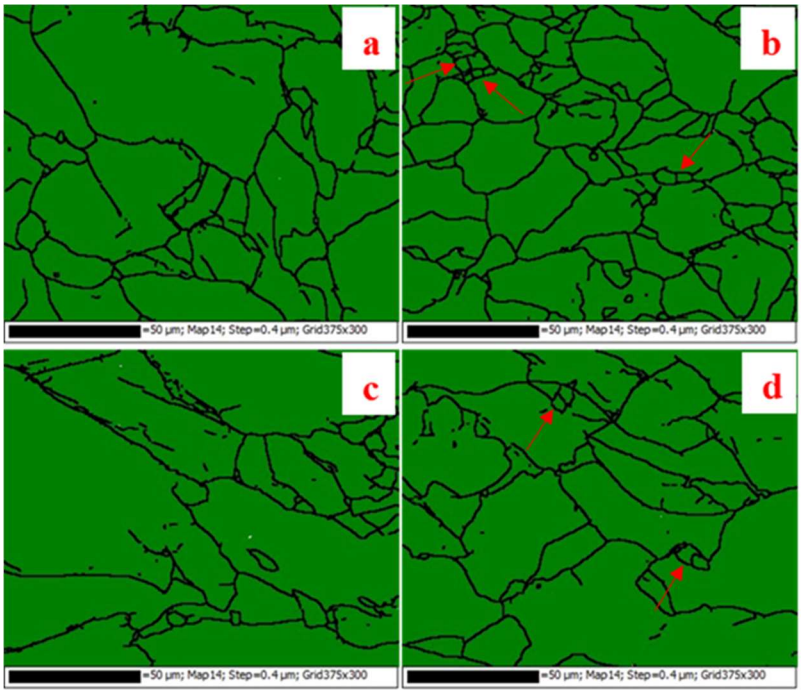

Figure 6. EBSD image at a step size of 0.4 µm for misorientations greater than 5° for (a) alloy-1 rolled at a temperature of 800 ℃; (b) alloy-1 rolled at a temperature of 850 ℃, the recrystallized grains are shown by red arrows; (c) alloy-2 rolled at a temperature of 800 ℃ and (d) alloy-2 rolled at a temperature of 850 ℃, the recrystallized grains are shown by red arrows.

It was found that the alloy-2 exhibited a marginally higher mean low angle grain boundaries

misorientation when it was rolled at a lower temperature of 800 ℃ as shown in Figures 5 and, 7c,d. There were relatively higher fractions of high angle grain boundaries was present in alloy-1 (Figures 7a,b) as compared to alloy-2 (Figures 7c,d). In context to high angle grain boundaries the complimentary low angle grain boundaries fractions were less, therefore the mean low angle grain boundaries were lower for alloy-2 as compared to alloy-1 which is already depicted in Figure 5. It was suggested that the formation of titanium carbide/Nitride in the alloy-2 was served as a high energy density site where the accumulation of sub-grains/sub-substructures/dislocations took place which overall increased the mean low angle grain boundaries percentage/fractions as compared to its counterpart (alloy-2) without havening titanium as micro-alloyed elements. Also, it was quite obvious that the solubility of titanium was higher during rolling at a higher temperature of 850 ℃, which reduced the extent of titanium carbide/nitride precipitations and hence a comparatively lower mean low angle misorientation angle was observed as shown in Figure 5.

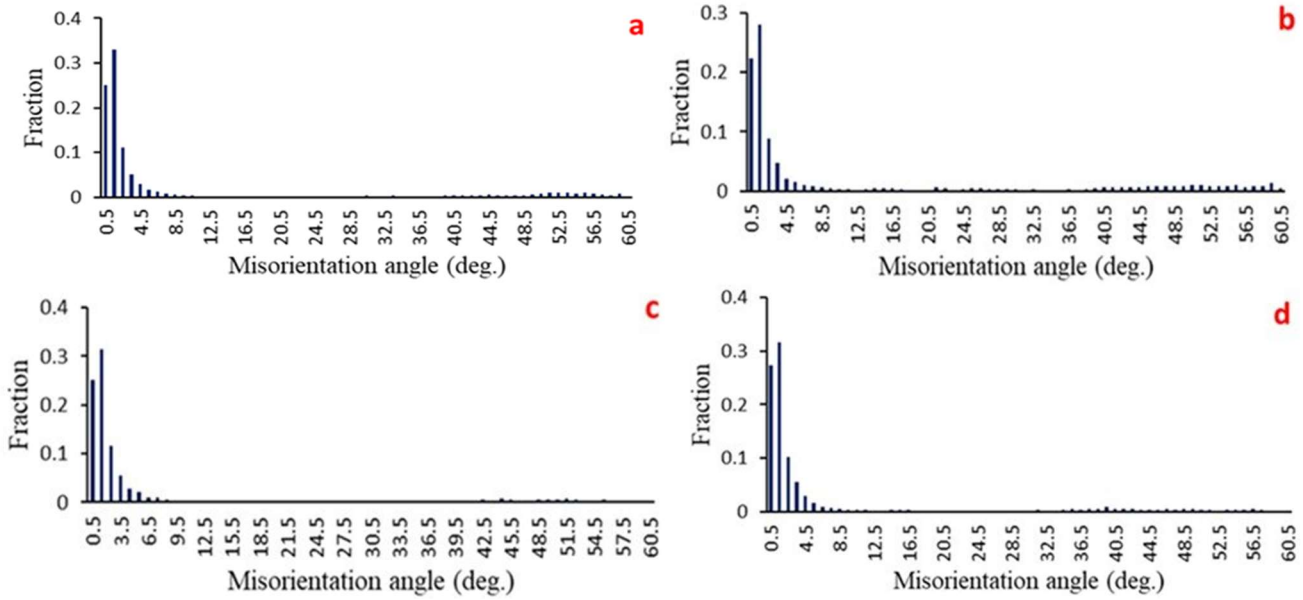

Figure 7. Misorientation angle distribution for (a) alloy-1 rolled at a temperature of 800 ℃; (b) alloy-1 rolled at a temperature of 850 ℃; (c) alloy-2 rolled at a temperature of 800 ℃ and (d) alloy-2 rolled at a temperature of 850 ℃.

3.4. Formation of precipitates

The TEM microstructure of alloy-1, when rolled at a temperature of 800 ℃, envisages sub-grains/sub-structures and precipitates formations as shown in Figures 8a,b; the substructures/precipitate size was observed in the order of nanometers. However, the microalloying element which envisages precipitates formation was not known therefore a spectroscopy analysis was done for the sample using "energy-dispersive X-ray" (EDXS). Figure 8d showed a peak of Cu along with very tiny peaks of oxygen (O) and silicon (Si). It suggested that the oxygen could not be contained in a nascent state and hence the precipitates formed in the microstructure were copper and oxy-silicates of Fe/Mn. The selected area diffraction pattern (SADP) showed that both matrix and precipitates spot as shown in Figure 8c. It is suggested that the precipitate was in body central cubic (bcc) in the bcc matrix of ferrite grain. The transmission electron microscopy image of alloy-2 when it was rolled at a

temperature of 800 ℃ is shown in Figure 9. The formation of precipitates/substructures was observed as shown in Figures 9a,b. It is suggested that these precipitates/substructures were formed along the rolling direction as evident from Figure 9a. However, the EDXS analysis also confirmed the peaks of copper with tiny peaks of titanium (Ti) and sulphur (S) as shown in Figure 9d. Therefore, it is suggested that the precipitates of Cu and Ti were formed along with other microalloying elements in combination. The darkfield SADP image in Figure 9c also confirms the formations of precipitates at the grain/sub-grain boundaries.

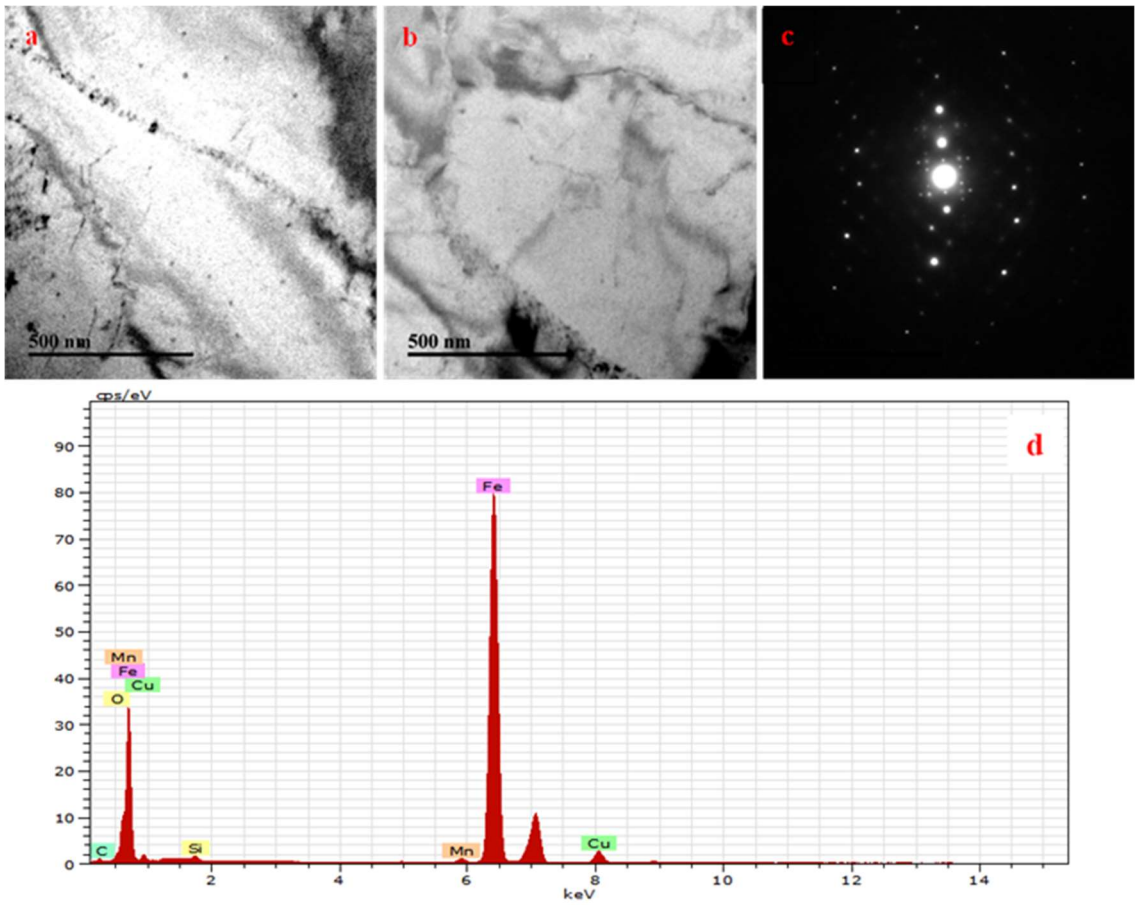

Figure 8. TEM microstructure of alloy-1 rolled at a temperature of 800 ℃ showing (a) sub-grains/substructures (b) precipitates around grain boundaries and (c) selected area diffraction pattern and (d) Energy-dispersive X-ray spectroscopy.

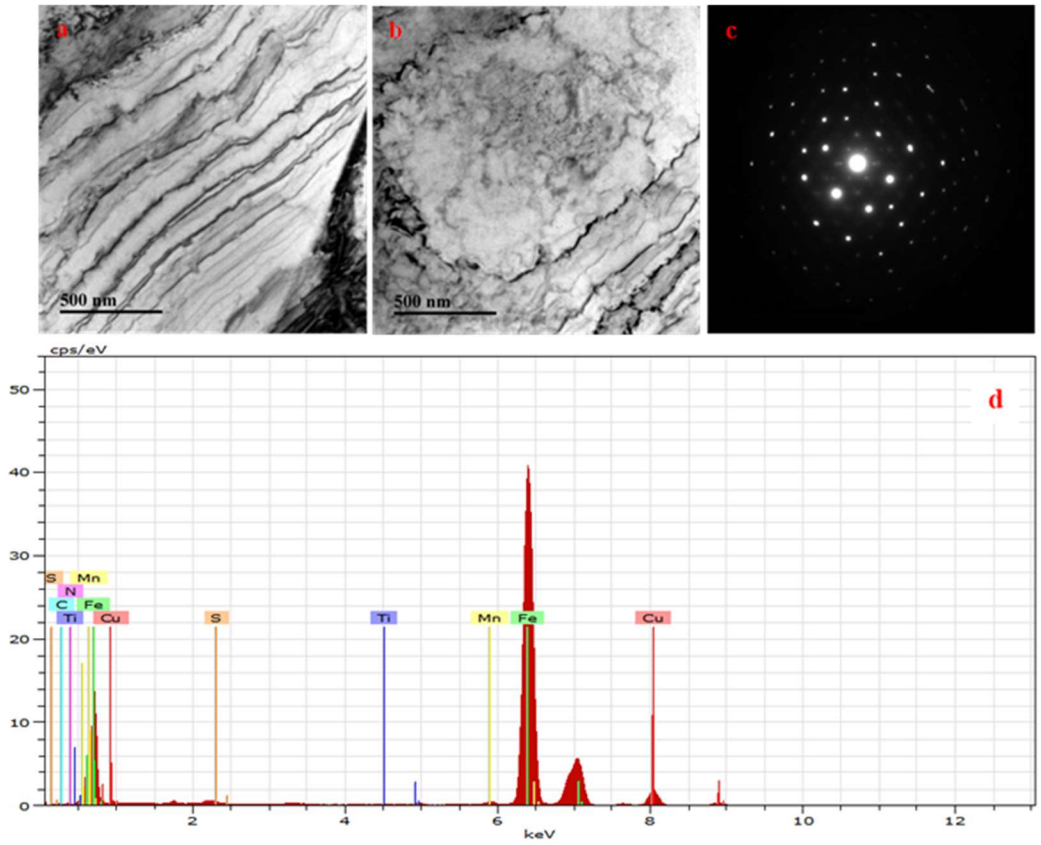

Figure 9. TEM microstructure of alloy-2 rolled at a temperature of 800 ℃ showing (a) sub-grains/substructures (b) precipitates around grain boundaries and (c) selected area diffraction pattern and (d) Energy-dispersive X-ray spectroscopy.

When the alloy-1 was rolled at a higher temperature of 850 ℃, the substructures/dislocations formation along with sub-grain/grain was observed. The substructure size was in the order of nanometer as shown in Figure 10a. There were few sites where the dislocations formed in a more abundant manner which is suggested to be the higher energy density sites. It was also once again confirmed the formation of coherent precipitates as shown in darkfield SADP (Figure 10b). The EDXS analysis showed the peaks of Cu with tiny pics of Cu, Mn, Si and oxygen suggesting the formation of their precipitates as shown in Figure 10c. The alloy-2, when rolled at a higher temperature of 850 ℃, the equisized fine precipitates were observed as shown in Figure 11a. The same is also depicted in the darkfield SADP image in Figure 11b. The EDXS analysis also confirms the presence of peaks of copper, titanium, sulphur and manganese (Figure 11c). It was also observed that these precipitates are much finer than what we observed when the same alloy was rolled at a lower temperature. It is suggested that these precipitates coprecipitated at a high temperature during solidification. These precipitates which formed at the grain/sub-grain interior have the potential to hinder the grain/sub-grain growth and provide stable sub-structures, however, this proposed theory may be verified in future work.

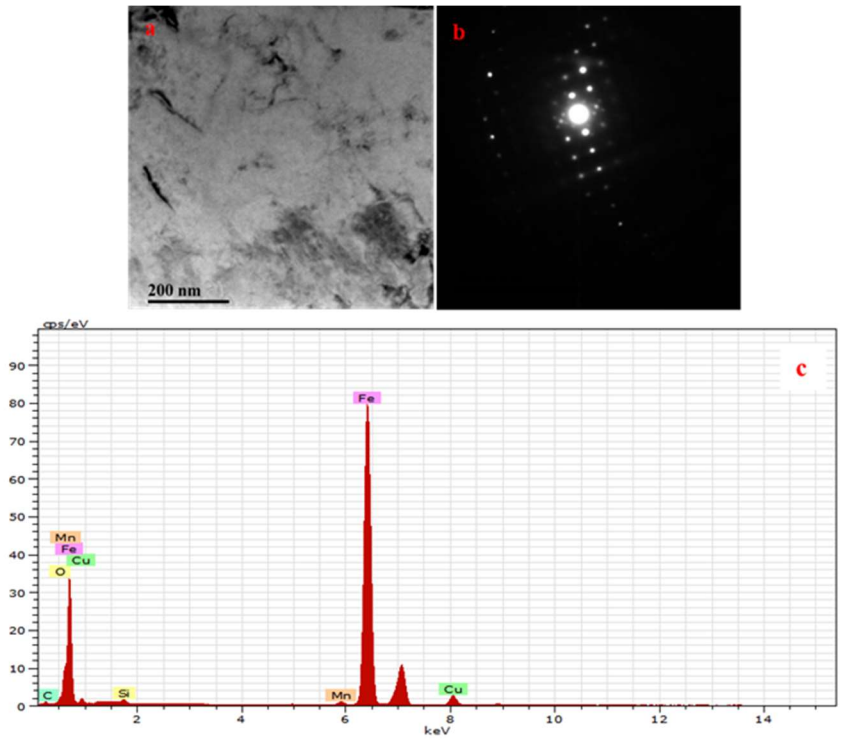

Figure 10. The TEM microstructure when alloy-1 was rolled at a higher temperature of 850 ℃ show (a) dislocations formation along with sub-grain/grain in the order of nano meters and (b) coherent precipitate in SADP and (c) Energy-dispersive X-ray spectroscopy.

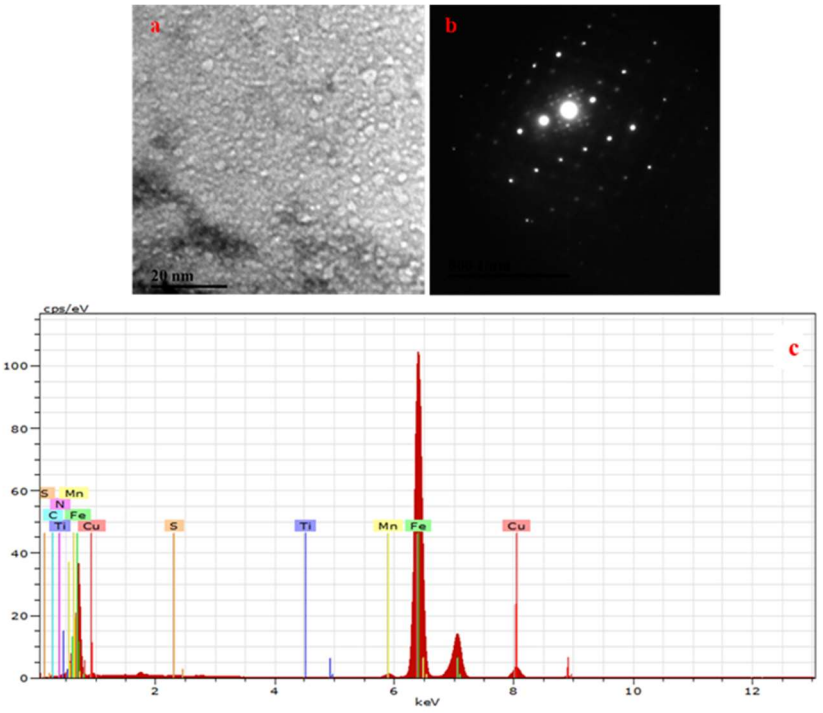

Figure 11. TEM microstructure of alloy-2 when rolled at a higher temperature of 850 ℃ showing (a) equisized fine precipitates and (b) coherent precipitates in SADP and (c) Energy-dispersive X-ray spectroscopy.

4. Conclusions

The principal idea of the present exertion produces distinguished conclusions which are briefly summarized below:

1. The EBSD microstructural analysis shows that the 0.05C–1.52Cu–1.45Mn stainless steel when subjected to hot rolling at a lower temperature envisaged a deformed microstructure rather transformed one. However, the same steel at a higher temperature envisages a transformed microstructure. There was no variation in hardness was observed. However, the addition of 0.05 wt% of titanium in 0.05C–1.52Cu–1.45Mn stainless steel influenced the softening and the hardness was decreased with the increasing rolling temperature because the solubility of titanium in the austenite phase increased with temperature which leads to suppression austenitic grain/sub-grain growth and hardness.

2. The 0.05C–1.52Cu–1.45Mn and 0.05C–0.05Ti–1.52Cu–1.45Mn stainless steel when subjected to rolling at a lower temperature, it was their ferrite/two-phase region which envisages work hardening/warm working. However, at a higher temperature, the quenching envisages a phase transformation leading to the elimination of deformed microstructure. The microstructure showed some recrystallization. It is suggested that these recrystallized grains were formed due to the restoration of the deformed microstructure generated during the rolling process at a higher temperature.

3. The mean sub-grain size for 0.05C–1.52Cu–1.45Mn stainless steel was 2.75 μm. However, the addition of titanium leads to a decrease in the mean sub-grain size. However, a marginally larger mean sub-grain size was observed when 0.05C–0.05Ti–1.52Cu–1.45Mn stainless steel was rolled at a higher temperature.

4. The 0.05C–1.52Cu–1.45Mn stainless steel when rolled at a lower temperature envisages sub-grains/sub-structures and precipitates formations. The substructures/precipitate size was observed in the order of nanometers. The "energy-dispersive X-ray spectra" (EDXS) showed a peak of Cu along with very tiny peaks of oxygen (O) and silicon (Si) which indicated that the precipitates formed in the microstructure were copper and oxy-silicates of Fe/Mn. It is suggested that the precipitate was in body central cubic (bcc) in the bcc matrix of ferrite grain. The further addition of titanium envisages the precipitate formation of titanium, copper and sulphides of Fe at the grain/sub-grain boundaries. However, when the same material was rolled at a higher temperature, the precipitates formed were much finer than what we observed when the same alloy was rolled at a lower temperature. It is suggested that these precipitates coprecipitated at a high temperature during solidification. Therefore, these precipitates may have the potential to hinder the grain/sub-grain growth and provide stable sub-structures, however, this proposed theory needs further verification and may be done in future work.

Conflicts of interest

The authors declare no conflict of interest.

References

1. Krishnadev MR, Galjbois (1975) Some aspects of precipitation of copper and columbium (Nb) carbide in an experimental high strength steel. *Metall Trans A* 6: 222–223. https://doi.org/10.1007/BF02673694

2. Tagawa H, Kurihara M, Abe T, et al. (1987) Development of YS460MPa grade steel plate for offshore structures with thermo-mechanically processed copper bearing age hardenable steel. *Trans IronSteelInst Jpn* 27: 478–484. https://doi.org/10.2355/isijinternational1966.27.478
3. Maruyama N, Sugiyama M, Hara T, et al. (1999) Precipitation and phase transformation of copper particles in low alloy ferritic and martensitic steels. *Mater Trans* 40: 268–277. https://doi.org/10.2320/matertrans1989.40.268
4. Kishida K, Akisue O (1990) Effect of copper content on mechanical properties of continuously annealed extra-low-carbon titanium-added steel sheets. *Tetsu To Hagane* 76: 759–766. https://doi.org/10.2355/tetsutohagane1955.76.5_759
5. Morita M, Sato K, Hosoya Y (1994) Effects of Cu and Ti–precipitates on recrystallization texture of Cu–precipitation hardening ultra low carbon cold-rolled steel sheet. *Tetsu To Hagane* 80: 48–53. https://doi.org/10.2355/tetsutohagane1955.80.1_48
6. Phaniraj MP, Shin YM, Lee J, et al. (2015) Development of high strength hot rolled low carbon copper-bearing steel containing nanometer sized carbides. *Mater Sci Eng A* 633: 1–8. https://doi.org/10.1016/j.msea.2015.02.067
7. Leslie WC (1981) Interstitial atoms in alpha iron, In: Leslie WC, *The Physical Metallurgy of Steels*, Washington: New York: McGraw-Hill, 85–91.
8. Pickering FB (1983) *Physical Metallurgy and The Design of Steels*, Inglaterra: Applied Science.
9. Huang KE, Logé RE (2016) A review of dynamic recrystallization phenomena in metallic materials. *Mater Des* 111: 548–574. https://doi.org/10.1016/j.matdes.2016.09.012
10. Rios PR, Siciliano Jr F, Sandim HR, et al. (2005) Nucleation and growth during recrystallization. *Mater Res* 8 225–238. https://doi.org/10.1590/S1516-14392005000300002
11. Zambrano PC, Guerrero MP, Colas R, et al. (2001) Microstructural analysis of hot-rolled, low-carbon steel strips. *Mater Charact* 47: 275–282. https://doi.org/10.1016/S1044-5803(01)00188-7
12. Funakawa Y, Shiozaki T, Tomita K, et al. (2004) Development of high strength hot-rolled sheet steel consisting of ferrite and nanometer-sized carbides. *ISIJ Int* 44: 1945–1951. https://doi.org/10.2355/isijinternational.44.1945
13. Misra RD, Jia Z, O'Malley R, et al. (2011) Precipitation behavior during thin slab thermomechanical processing and isothermal aging of copper-bearing niobium-microalloyed high strength structural steels: The effect on mechanical properties. *Mater Sci Eng A* 528: 8772–8780. https://doi.org/10.1016/j.msea.2011.08.047
14. Hwang B, Lee CG, Lee TH (2010) Correlation of microstructure and mechanical properties of thermomechanically processed low-carbon steels containing boron and copper. *Metall Mater Trans A* 41: 85–96. https://doi.org/10.1007/s11661-009-0070-4
15. Kumar P, Hodgson P, Beladi H, et al. (2020) EBSD Investigation to study the restoration mechanism and substructural characteristics of 23Cr–6Ni–3Mo duplex stainless steel during post-deformation annealing. *Trans Indian Inst Met* 73: 1421–1431. https://doi.org/10.1007/s12666-020-01884-1
16. Kumar P, Hodgson P, Beladi H, et al. (2021) Restoration mechanism and sub-structural characteristics of duplex stainless steel with an initial equiaxed austenite morphology during post-deformation annealing. *Key Eng Mater* 882: 64–73. https://doi.org/10.4028/www.scientific.net/KEM.882.64

AIMS Press